Complex Formation between Magnesocene ($MgCp_2$) and NH_3: Implications for p-Type Doping of Group III Nitrides and the Mg Memory Effect

George T. Wang* and J. Randall Creighton

Sandia National Laboratories, P.O. Box 5800, MS-0601, Albuquerque, New Mexico 87185

Received: August 21, 2003

Magnesocene (biscyclopentadienylmagnesium) is a common precursor used for the p-type doping of GaN and other group III nitride materials. Unfortunately, difficulties remain with predictably controlling the incorporation of Mg during metal organic chemical vapor deposition (MOCVD) film growth, which often exhibits poorly understood "memory effects." Although the formation of a reaction product between magnesocene and ammonia has been previously speculated, one has never been experimentally isolated or identified. We have spectroscopically observed and identified, for the first time, the adducts formed between magnesocene and ammonia. Density functional theory (DFT) quantum chemistry calculations have also been performed on the system to determine the structures and energetics of the reaction products. It was found that ammonia can form condensable Lewis acid−base complexes with magnesocene in both 1:1 and 2:1 ratios (i.e., NH_3-MgCp_2 and $(NH_3)_2-MgCp_2$) via nucleophilic attack of NH_3 at the positively charged Mg center of $MgCp_2$. Adduct formation is reversible, and the 1:1 and 2:1 products can be converted to one another by controlling the NH_3 partial pressure. The formation and condensation of both adducts at room temperature is the probable parasitic source that leads to many of the observed Mg incorporation difficulties during the p-type doping of group III nitride materials.

Introduction

The group III nitrides, including GaN and its alloys with AlN and InN, have a number of properties, including a direct, wide band gap, high thermal conductivity, and high thermal stability, that make them attractive for use in optoelectronic devices as well as in high-power and high-temperature electronic devices. As a result, the group III nitrides have been among the most heavily studied electronic materials over the past decade and have been successfully commercialized. For the p-type doping of GaN and its alloys, the dominant species employed is magnesium, which is typically delivered during metal organic chemical vapor deposition (MOCVD) via the organometallic precursor magnesocene ($MgCp_2$) (Cp = cyclopentadienyl group). Unfortunately, controlled incorporation of magnesium into III nitride films has been difficult. Often the result from p-type doping is unpredictable Mg concentration profiles that may vary significantly from run to run. Even in reactors in which the Mg doping process is reproducible, the Mg in the grown films is marked by broad concentration profiles corresponding to a slow response in the doping turn-on and turn-off sequence. This issue, sometimes referred to as a magnesium "memory effect,"[1−4] is problematic because tight control of doping profiles is required for optimal device performance.

In group II metallocenes, it is typical to denote the charge distribution as $M^{2+}(Cp^-)_2$. Previous calculations using atoms in molecules (AIM) theory on $MgCp_2$ have supported this description of a large degree of Mg−Cp charge separation, with approximate charges on the Mg and Cp ligands of +1.75 and −0.88, respectively.[5] The electron deficiency of the Mg center in $MgCp_2$ suggests that it may be susceptible to nucleophilic attack by NH_3, the primary nitrogen source used for group III nitride growth, to form a Lewis acid−base complex, as given in eq 1. Such a reaction between $MgCp_2$ and NH_3 could be the principal source of the magnesium doping issues that have been observed if adduct formation prevents or hinders magnesocene from reaching the growth surface. Previous work has reported solid particle formation in the gas phase resulting from the mixing of bismethylcyclopentadienylmagnesium ($Mg(MeCp)_2$) and ammonia,[6] suggesting that $MgCp_2$ and NH_3 may also react together in the gas phase at room temperature. Xia et al. have recently observed adducts of $MgCp_2$ with various primary and secondary amines in solution.[7]

$$MgCp_2 + NH_3 \leftrightarrow NH_3-MgCp_2 \quad (1)$$

Despite the importance of the p-type doping process and its various unresolved issues, the chemistry between ammonia and $MgCp_2$ has not been previously investigated to our knowledge. In this study, we have probed the interaction between ammonia and $MgCp_2$ using a combination of FTIR experiments performed under a typical MOCVD environment and density functional theory (DFT) quantum chemistry calculations. In addition to the 1:1 NH_3-MgCp_2 adduct considered in reaction 1, we also consider in this work the reaction in which a second NH_3 molecule initiates nucleophilic attack at the Mg atom of the NH_3-MgCp_2 adduct to form a 2:1 $(NH_3)_2-MgCp_2$ adduct, as shown in eq 2.

$$NH_3-MgCp_2 + NH_3 \leftrightarrow (NH_3)_2-MgCp_2 \quad (2)$$

From the theoretical and experimental results of this work, we propose in this paper a model for the interaction of $MgCp_2$ and NH_3 as follows:

$$MgCp_2 + 2NH_3 \leftrightarrow NH_3-MgCp_2 + NH_3 \leftrightarrow (NH_3)_2-MgCp_2 \quad (3)$$

* Corresponding author. E-mail: gtwang@sandia.gov.

10.1021/jp036494e CCC: $27.50
Published on Web 05/04/2004

Our results show that $MgCp_2$ and NH_3 undergo facile complexation reactions at room temperature and that the condensation of these adducts onto reactor surfaces is the likely cause of the Mg doping issues.

Theoretical and Experimental Methods

Main-group chemistry has been widely studied using density functional theory (DFT) methods. DFT calculations using the B3LYP hybrid functional[8] were employed in this study to examine the chemistry between magnesocene and NH_3. The Gaussian 98 software package[9] was used for all of the calculations. Geometry optimizations were carried out without symmetry constraints using the 6-31G(d) basis set in order to locate the stationary points on the potential energy surface. Frequency calculations using the 6-31G(d) basis set were performed for each stationary point to obtain the zero-point energies, thermal corrections, and infrared frequencies. The calculated stationary points on the potential energy surface were verified by an analysis of the normal modes as either minima by the presence of no imaginary frequencies or as transition states by the presence of exactly one imaginary frequency. Because single-point energies are known to be more sensitive to basis-set size than geometry optimizations or frequency calculations, the energies of the stationary points on the potential energy surface were calculated using the 6-311+G(d,p) and 6-311+G(3df,2p) basis sets in addition to the 6-31G(d) basis set. Single-point energies run using the 6-311+G(3df,2p) basis set were calculated using SCF = tight convergence criteria in Gaussian 98. All energies reported in this paper have been zero-point corrected.

In situ Fourier transform infrared spectroscopy (FTIR) experiments were performed to probe the interaction between magnesocene and ammonia. Gases were introduced into a stainless steel cell at room temperature, simulating cold-wall reactor inlet conditions. The cell was constructed of standard vacuum components, equipped with KBr windows, and resided in the FTIR sample compartment. A KCl substrate (3 mm thick) was located near the point where magnesocene and ammonia mixing occurred, so the transmission spectrum for any condensable product could be measured. Because of the short path length (~7 cm), gas-phase IR absorption was relatively weak and could be removed by ratioing against the appropriate reference spectrum (e.g., that of pure NH_3). Spectra were collected from 500 to 4000 cm^{-1} with 2-cm^{-1} resolution.

Magnesocene was delivered using a standard bubbler configuration, with H_2 as the carrier gas. A bubbler H_2 flow rate of 500 sccm corresponds to a $MgCp_2$ flow of 0.79 μmol/min using the reported $MgCp_2$ vapor-pressure curve from Lewis et al.[10] The total H_2 flow rate (including the $MgCp_2$ bubbler flow) was 6000 sccm, and the ammonia flow rate was varied from 0 to 1000 sccm. The total pressure in the cell was controlled from 20 to 500 Torr with a downstream throttle valve. It should be noted that at constant input flow rates the $MgCp_2$ and NH_3 concentrations scale with the total pressure.

Theoretical Results

The fully optimized geometries of the species considered in this work are shown in Figure 1. Calculated energies of the optimized structures relative to the reactants are given in Table 1. It can be seen in Table 1 that the calculated single-point energies are sensitive to the basis set size. Energies reported in this paper will refer to single-point energies calculated using the largest 6-311+G(3df,2p) basis set used. Selected bond lengths and angles of interest for the optimized structures shown in Figure 1 are given in Table 2.

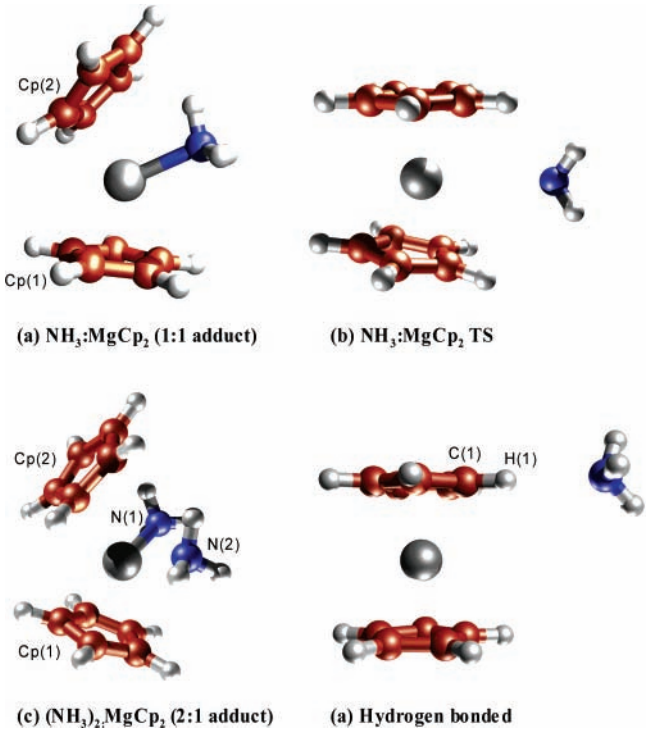

Figure 1. Optimized geometries of (a) NH_3-MgCp_2, (b) the NH_3-MgCp_2 transition state, (c) $(NH_3)_2-MgCp_2$, (d) NH_3 hydrogen bonded to $MgCp_2$. Red, gray, and blue atoms represent C, Mg, and N, respectively.

TABLE 1: Calculated Relative Energies (kcal/mol) of the Species Considered in This Work

	6-31G(d)	6-311+G(d,p)	6-311+G(3df,2p)
NH_3-MgCp_2	−10.1	−6.9	−5.4
NH_3-MgCp_2 TS	−1.1	0.6	1
$(NH_3)_2-MgCp_2$	−21.6	−14.9	−12.3
H-bonded	−1.7	−0.8	−0.1

TABLE 2: Selected Calculated Bond Lengths (Å) and Angles (deg) for Species Considered in This Work

$MgCp_2$		$(NH_3)_2-MgCp_2$	
Cp−Mg−Cp	178.7	Cp−Mg−Cp	144.1
Mg−Cp	2.030	Mg−N(1)	2.170
		Mg−N(2)	2.210
NH_3-MgCp_2		N(1)−Mg−N(2)	92.9
Cp−Mg−Cp	157.3	Mg−Cp(1)	2.175
Mg−N	2.149	Mg−Cp(2)	2.789
Mg−Cp(1)	2.095		
Mg−Cp(2)	2.565		
NH_3-MgCp_2 TS		hydrogen bonded	
Cp−Mg−Cp	167.8	Cp−Mg−Cp	178.4
Mg−N	3.723	N−H(1)	2.476
Mg−Cp(1)	2.045	C(1)−H(1)	1.10
Mg−Cp(2)	2.104		

The equilibrium structure for the 1:1 NH_3-MgCp_2 adduct is shown in Figure 1a. Complex formation is energetically favorable, with a calculated binding energy of 5.4 kcal/mol. Mg−N bond formation is evident, with a calculated Mg−N distance of 2.15 Å. The weak binding energy indicates donor−acceptor rather than strong covalent Mg−N bond formation. It can be seen in Figure 1a that magnesocene has been distorted from its linear equilibrium geometry to a bent geometry upon complexation with NH_3, with a calculated Cp−Mg−Cp angle (where Cp denotes the ring centroid) of 157.3°. Adduct

formation causes a significant increase in the Mg−Cp distance, to 2.57 from 2.03 Å in $MgCp_2$, for one of the cyclopentadienyl rings. The result is a change in the hapticity of the ring from η^5 to η^2, with the Mg−C distance for three of the ring carbons equal to or greater than 3.0 Å in the 1:1 adduct. For the other Cp ring, the Mg−Cp distance increases only slightly to 2.10 Å and maintains a hapticity of η^5.

The bent geometry of NH_3-MgCp_2 suggests that a barrier associated with a change from the linear geometry of $MgCp_2$ may be required for complex formation. Blom et al.[11] previously calculated that approximately 3.5 kcal/mol was required to bend $MgCp_2$ from 180 to 160° (Cp−Mg−Cp). We were able to locate a transition state for the complexation reaction, which is shown in Figure 1b. An analysis of the imaginary normal mode of the transition state confirms that it is associated with the bending of $MgCp_2$ from its linear geometry. The energy of the transition state relative to the reactants was found to be only 1.0 kcal/mol, indicating that adduct formation should be facile at room temperature.

The equilibrium structure of the 2:1 $(NH_3)_2-MgCp_2$ adduct, formed by the nucleophilic attack of the 1:1 NH_3-MgCp_2 adduct by an additional NH_3 molecule, is shown in Figure 1c. The formation of the 2:1 adduct is energetically favorable compared to that of the 1:1 NH_3-MgCp_2 adduct and has a calculated binding energy of 12.3 kcal/mol. Interestingly, the nucleophilic attack of the second NH_3 molecule at Mg leads to a greater change in the energy (−6.9 kcal/mol relative to that of the 1:1 adduct) than the initial attack of the first NH_3 molecule to form the 1:1 adduct (−5.4 kcal/mol). This may be due to a preferred coordination state of the Mg atom in $(NH_3)_2-MgCp_2$ versus NH_3-MgCp_2. No transition state could be located for the formation of $(NH_3)_2-MgCp_2$ from the reaction of NH_3 and NH_3-MgCp_2, implying that no barrier or only an insignificant barrier exists for this process. Thus, the formation of $(NH_3)_2-MgCp_2$ is predicted to be facile at room temperature. The formation of $(NH_3)_2-MgCp_2$ further increases the bend of $MgCp_2$, with a decrease in the Cp−Mg−Cp angle to 144.1 from 157.3° in NH_3-MgCp_2. The ring centroid-to-Mg distances are also increased to 2.18 and 2.79 from 2.10 and 2.57 Å, respectively, in the 1:1 adduct, indicating weaker ring−Mg interactions in the 2:1 adduct. The Mg−N bond lengths in the 2:1 adduct are not equivalent, at 2.17 and 2.21 Å, and are slightly longer than the 2.15-Å Mg−N bond in the 1:1 adduct.

We have also considered the possibility of a hydrogen bonding interaction between the Cp ring hydrogens with ammonia. Figure 1d shows the optimized geometry of NH_3 hydrogen bonded to a ring hydrogen of $MgCp_2$. An analysis of the calculated vibrational normal modes of the hydrogen-bonded adduct shows a stretching mode between NH_3 and the nearest ring hydrogen at 74.5 cm^{-1} (unscaled). However, the binding energy of the hydrogen-bonded adduct was calculated to be only 0.1 kcal/mol. Because of this insignificant binding energy, it is unlikely that the hydrogen-bonded adduct will be observed experimentally at room temperature. Xia et al. recently reported intramolecular and intermolecular hydrogen bonding between the cyclopentadienyl rings of $MgCp_2$ and the hydrogens of various primary and secondary amines.[7] An analysis of the calculated normal modes of NH_3-MgCp_2 and $(NH_3)_2-MgCp_2$ indicates that the lowest-frequency ν(N−H) mode for each adduct is associated with the ammonia hydrogen closest to a cyclopentadienyl ring. This suggests intramolecular hydrogen bonding interactions in both the 1:1 and 2:1 adducts of NH_3 and $MgCp_2$.

FTIR Results

The introduction of $MgCp_2$ or NH_3 separately into the IR cell at room temperature does not result in any detectable buildup of condensable species on the internal KCl window. However, when the cell is filled with both $MgCp_2$ and NH_3 at room temperature, the buildup of a hazy, white film on the KCl observable to the naked eye is seen, indicating the formation of a condensable product between $MgCp_2$ and NH_3. IR data taken at different process conditions show that similar but distinct products can be formed by mixing $MgCp_2$ and NH_3 in the gas phase at room temperature—one corresponding to low-pressure growth and one corresponding to high-pressure growth.

Figure 2 shows the IR spectrum of the condensable product observed following the introduction of both magnesocene and ammonia at a total pressure of 20 Torr and flows of 800 sccm of NH_3 and 500 sccm of H_2 through the $MgCp_2$ bubbler. The spectrum was taken after an arbitrary amount of film growth, which continues indefinitely as long as both sources are present. The IR spectrum of the condensed film taken at a higher total pressure of 500 Torr and flows of 1000 sccm of NH_3 and 500 sccm of H_2 through the $MgCp_2$ bubbler is shown in Figure 3. The low-pressure and high-pressure spectra, although distinct, both contain peaks in the same frequency ranges that correspond to modes that would be consistent with adducts containing $MgCp_2$ and NH_3. Although there is considerable overlap between both spectra, the low-pressure spectrum in Figure 2 exhibits a strong peak a 773 cm^{-1} that is absent from the high-pressure spectrum (Figure 3). Likewise, the high-pressure spectrum contains a peak at 689 cm^{-1} that is not present to any significant degree in the low-pressure spectrum. This indicates that the 20-Torr and 500-Torr data in Figures 2 and 3, respectively, represent distinct products, with no significant amount of the high-pressure product being present at low pressure and vice versa.

The assignment of the products observed in Figures 2 and 3 can be made by considering the equilibrium relation given by eq 3. Because of the low concentration of $MgCp_2$, NH_3 is always present in large excess. An increase in pressure will have the effect of increasing the NH_3 partial pressure, thus shifting the reaction equilibrium to the right, from the 1:1 adduct to the 2:1 adduct. Therefore, we assign the low-pressure product in Figure 2 to the 1:1 NH_3-MgCp_2 complex and the high-pressure product in Figure 3 to the 2:1 $(NH_3)_2-MgCp_2$ complex.

This assignment can be verified by the changes observed in the IR spectra when the NH_3 partial pressure is altered after the growth of the high-pressure product (i.e, the 2:1 adduct) while maintaining a total pressure of 500 Torr. Figure 4a shows the 2:1 adduct formed at a total pressure of 500 Torr from $MgCp_2$ bubbler and NH_3 flows of 500 and 1000 sccm, respectively. In Figure 4a, the $MgCp_2$ flow has been turned off, which arrests further film growth but does not result in the loss of the condensed product. Figure 4b shows that when the NH_3 flow is shut off the film converts to a product with an IR signature virtually identical in shape to the low-pressure adduct shown in Figure 2. This verifies that the low-pressure product is the same as that observed when the NH_3 partial pressure is reduced at high pressure (i.e., the 1:1 adduct). This conversion of $(NH_3)_2-MgCp_2$ to NH_3-MgCp_2 is captured in Figure 4c (the difference spectrum of Figure 4b and a), which shows the appearance of 1:1 adduct features and the loss of 2:1 adduct peaks. Figure 4b (and hence Figure 4c) was taken within a couple of minutes after turning the NH_3 flow off and thus shows that the conversion of the 2:1 adduct to the 1:1 adduct occurs on a relatively fast time scale. When the NH_3 is turned back on

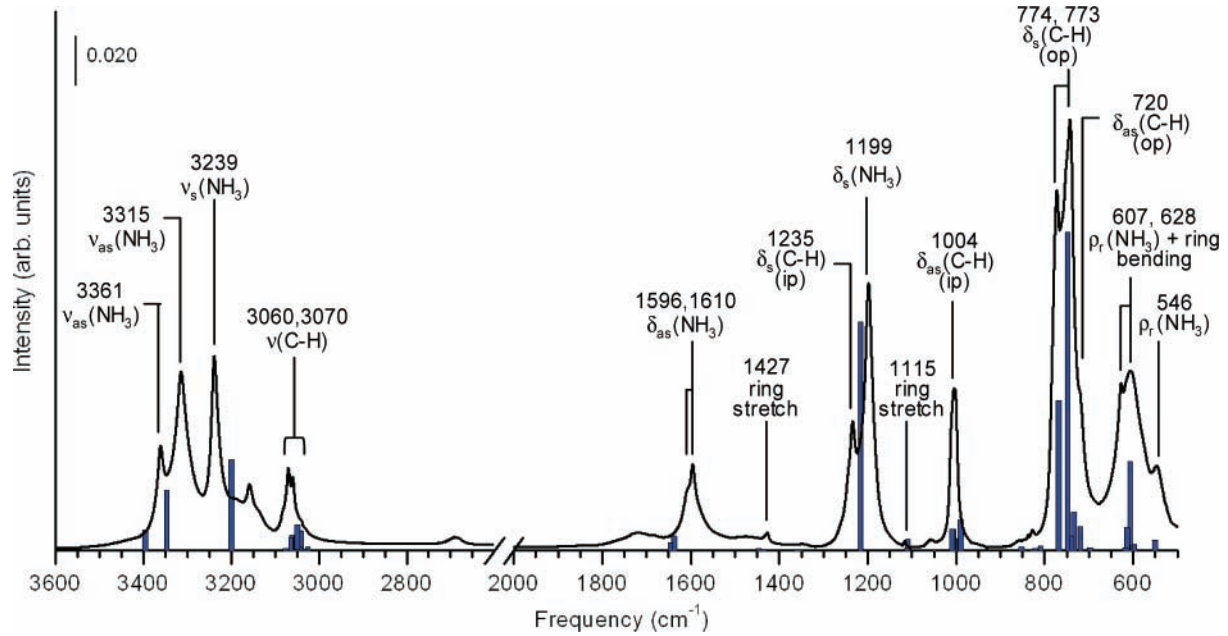

Figure 2. Infrared spectrum taken during the growth of the condensable product of $MgCp_2$ and NH_3 at a total pressure of 20 Torr. $MgCp_2$ bubbler and NH_3 flows were 500 and 800 sccm, respectively. Rectangular bars represent the calculated spectrum for NH_3-MgCp_2 (the 1:1 adduct). A scaling factor of 0.97 was employed, except for the C−H and N−H stretching modes, for which a scaling factor of 0.947 was used.

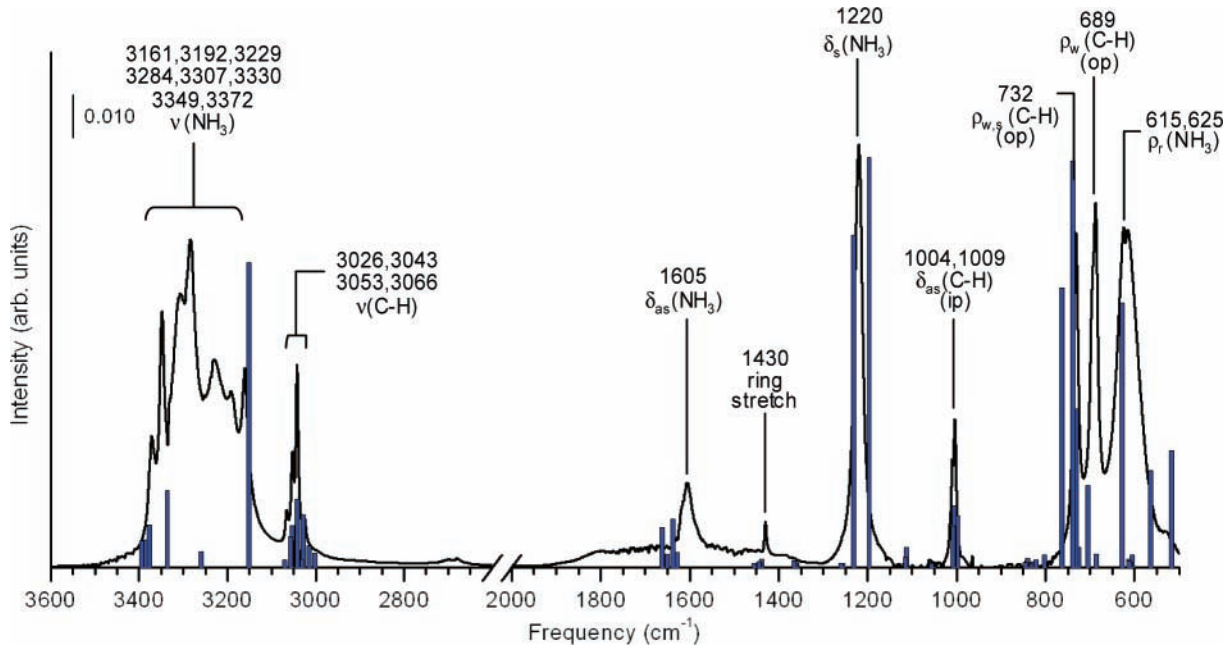

Figure 3. Infrared spectrum taken during the growth of the condensable product of $MgCp_2$ and NH_3 at a total pressure of 500 Torr. $MgCp_2$ bubbler and NH_3 flows were 500 (in H_2 carrier gas) and 1000 sccm, respectively. Rectangular bars represent the calculated spectrum for $(NH_3)_2-MgCp_2$ (the 2:1 adduct). A scaling factor of 0.97 was employed, except for the C−H and N−H stretching modes, for which a scaling factor of 0.947 was used.

at the same flow rate of 1000 sccm (with the $MgCp_2$ flow still shut off), the film converts back to the 2:1 adduct, as shown in Figure 4d. If the NH_3 is turned off again, then the film converts back to the 1:1 adduct and decreases in intensity over a period of several minutes by dissociation, desorption, or a combination of both. Eventually, no significant trace of the film is observed, as shown in Figure 4e, indicating that the reaction of $MgCp_2$ and NH_3 is entirely reversible at room temperature.

This observed chemistry of the condensed products as the NH_3 flow is turned off and on is entirely consistent with the proposed model given in eq 3 and verifies that both 1:1 and 2:1 adducts can be formed at a given pressure (although not necessarily at any pressure) by adjusting the NH_3 partial pressure. Increasing the NH_3 concentration shifts the equilibrium toward the 2:1 $(NH_3)_2-MgCp_2$ adduct. Decreasing the NH_3 concentration shifts the equilibrium to the left, to the 1:1 NH_3-MgCp_2 adduct and the reactants. The low-pressure and high-pressure products shown in Figures 2 and 3 simply represent growth conditions in which the equilibrium is shifted to the 1:1 and 2:1 adducts, respectively. We note that the reactions are entirely reversible at room temperature and support the assignment of the products of $MgCp_2$ and NH_3 to Lewis acid−base complexes with binding energies in the neighborhood of those predicted by the theoretical calculations. The results of this study also suggest that the solid particles that were observed by

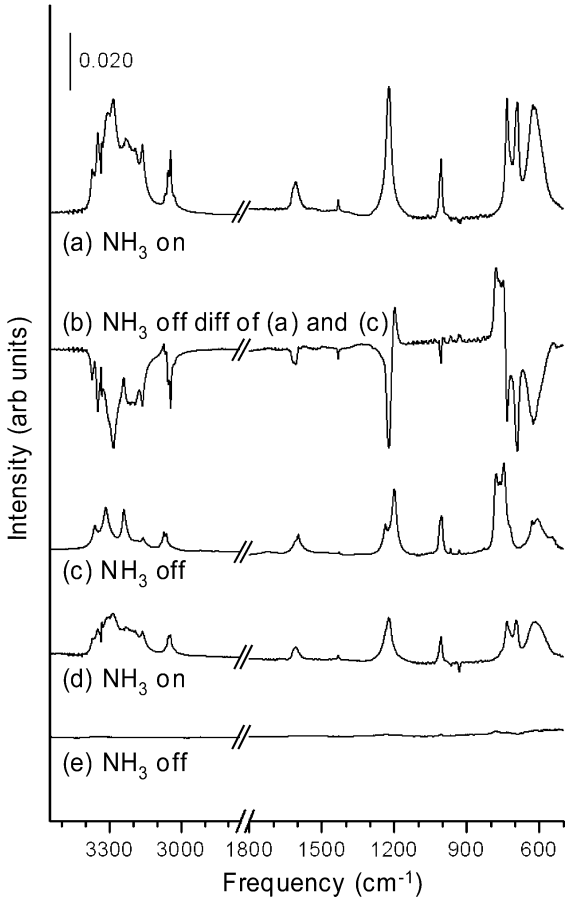

Figure 4. Infrared spectra after film growth probing the effect of NH_3 partial pressure at a fixed total pressure of 500 Torr. Spectra were taken in the absence of $MgCp_2$ flow, which was turned off prior to scanning. NH_3 on and off states represent 1000 and 0 sccm, respectively. Spectra are listed in chronological order: (a) NH_3 flow on; (b) difference between a and c; (c) NH_3 flow turned off; (d) NH_3 flow turned back on; (e) NH_3 flow turned off after several minutes.

Haffouz et al.[6] to form between $MeMgCp_2$ and NH_3 were Lewis acid−base complexes and not elimination products as previously proposed.

The calculated IR spectra for the 1:1 and 2:1 adducts are shown as overlays on the low-pressure and high-pressure spectra in Figures 2 and 3, respectively. The calculated spectra are reasonably good fits with the experimental data and predict most of the major spectral features, further supporting the product assignments. However, because of the similarity in the 1:1 and 2:1 adducts, it is not unexpected that their calculated spectra are each acceptable fits with both the low pressure and high-pressure experimental spectra. Hence, the assignments of the 1:1 NH_3-MgCp_2 adduct to the products observed at low NH_3 partial pressures and the 2:1 $(NH_3)_2-MgCp_2$ adducts to the products observed at high NH_3 partial pressures are based on a combination of the experimental observations and theoretical predictions rather than solely on the fit of the calculated IR spectra.

Conclusions

The interaction of magnesocene and ammonia has been investigated at room temperature using a combination of FTIR experiments and DFT calculations to elucidate difficulties in incorporating Mg into group III nitrides during p-type doping. It was found that ammonia and magnesocene can form donor−acceptor complexes at room temperature in both 1:1 and 2:1 ratios (i.e., NH_3-MgCp_2 and $(NH_3)_2-MgCp_2$).

Both NH_3-MgCp_2 and $(NH_3)_2-MgCp_2$ were seen to be condensable at room temperature under reactant flow conditions typical of group III nitride MOCVD growth. We believe that the formation and subsequent condensation of these low-vapor-pressure adducts is a probable source of parasitic Mg loss that results in the observed unpredictable Mg incorporation and slow turn-on and turn-off response during p-type doping of group III nitrides. This points to two obvious paths to improve the Mg doping performance. The first is simply to prevent adduct formation from occurring. This can be achieved to some degree by avoiding mixing the $MgCp_2$ and NH_3 flows for as long as possible before the growth substrate is reached. However, because of the insignificant reaction barriers calculated for the formation of the complexes, some adduct formation is inevitable. Recognizing the fact that adduct formation will occur, the second option is to prevent or limit adduct condensation. That is, if the vapor pressures of the adducts are not exceeded, then condensation and hence parasitic loss of Mg will be avoided. This can be achieved by lowering the reactant flows (e.g., the NH_3 flow) or by heating the upstream reactor components to shift the equilibrium of the reaction back to the gas-phase reactants. Preliminary quartz crystal microbalance growth experiments indicate that this approach is effective at preventing the condensation of the complexes of $MgCp_2$ and NH_3.

Acknowledgment. Sandia is a multiprogram laboratory operated by Sandia Corporation, a Lockheed Martin Company, for the United States Department of Energy under contract DE-AC04-94AL85000. We especially acknowledge support from the Office of Basic Energy Sciences.

References and Notes

(1) Ohba, Y.; Hatano, A. *J. Cryst. Growth* **1994**, *145*, 214.
(2) Schurman, M. J.; Slagaj, T.; Tran, C.; Karlicek, R.; Ferguson, I.; Stall, R.; Thompson, A. *Mater. Sci. Eng., B* **1997**, *43*, 222.
(3) Xing, H. L.; Green, D. S.; Yu, H. J.; Mates, T.; Kozodoy, P.; Keller, S.; Denbaars, S. P.; Mishra, U. K. *Jpn. J. Appl. Phys., Part 1* **2003**, *42*, 50.
(4) Davis, R. F.; Roskowski, A. M.; Preble, E. A.; Speck, J. S.; Heying, B.; Freitas, J. A.; Glaser, E. R.; Carlos, W. E. *Proc. IEEE* **2002**, *90*, 993.
(5) Bytheway, I.; Popelier, P. L. A.; Gillespie, R. J. *Can. J. Chem.-Rev. Can. Chim.* **1996**, *74*, 1059.
(6) Haffouz, S.; Beaumont, B.; Leroux, M.; Laugt, M.; Lorenzini, P.; Gibart, P.; Hubertpfalzgraf, L. G. *MRS Internet J. N. S. R.* **1997**, *2*, 27.
(7) Xia, A. B.; Heeg, M. J.; Winter, C. H. *J. Am. Chem. Soc.* **2002**, *124*, 11264.
(8) Becke, A. D. *J. Chem. Phys.* **1993**, *98*, 5648.
(9) Frisch, M. J.; Trucks, G. W.; Schlegel, H. B.; Scuseria, G. E.; Robb, M. A.; Cheeseman, J. R.; Zakrzewski, V. G.; Montgomery, J. A., Jr.; Stratmann, R. E.; Burant, J. C.; Dapprich, S.; Millam, J. M.; Daniels, A. D.; Kudin, K. N.; Strain, M. C.; Farkas, O.; Tomasi, J.; Barone, V.; Cossi, M.; Cammi, R.; Mennucci, B.; Pomelli, C.; Adamo, C.; Clifford, S.; Ochterski, J.; Petersson, G. A.; Ayala, P. Y.; Cui, Q.; Morokuma, K.; Malick, D. K.; Rabuck, A. D.; Raghavachari, K.; Foresman, J. B.; Cioslowski, J.; Ortiz, J. V.; Stefanov, B. B.; Liu, G.; Liashenko, A.; Piskorz, P.; Komaromi, I.; Gomperts, R.; Martin, R. L.; Fox, D. J.; Keith, T.; Al-Laham, M. A.; Peng, C. Y.; Nanayakkara, A.; Gonzalez, C.; Challacombe, M.; Gill, P. M. W.; Johnson, B. G.; Chen, W.; Wong, M. W.; Andres, J. L.; Head-Gordon, M.; Replogle, E. S.; Pople, J. A. *Gaussian 98*, revision A.5; Gaussian, Inc.: Pittsburgh, PA, 1998.
(10) Lewis, C. R.; Dietze, W. T.; Ludowise, M. J. *J. Electron. Mater.* **1983**, *12*, 507.
(11) Blom, R.; Faegri, K.; Volden, H. V. *Organometallics* **1990**, *9*, 372.